CellPress
OPEN ACCESS

Trends in
Biochemical Sciences

Special Issue: Pushing boundaries of cryo-EM

Review

Structural basis of torque generation in the bi-directional bacterial flagellar motor

Haidai Hu [1], Mònica Santiveri [1], Navish Wadhwa [2,3], Howard C. Berg [2,3], Marc Erhardt [4], and Nicholas M.I. Taylor [1,*]

The flagellar stator unit is an oligomeric complex of two membrane proteins ($MotA_5B_2$) that powers bi-directional rotation of the bacterial flagellum. Harnessing the ion motive force across the cytoplasmic membrane, the stator unit operates as a miniature rotary motor itself to provide torque for rotation of the flagellum. Recent cryo-electron microscopic (cryo-EM) structures of the stator unit provided novel insights into its assembly, function, and subunit stoichiometry, revealing the ion flux pathway and the torque generation mechanism. Furthermore, *in situ* cryo-electron tomography (cryo-ET) studies revealed unprecedented details of the interactions between stator unit and rotor. In this review, we summarize recent advances in our understanding of the structure and function of the flagellar stator unit, torque generation, and directional switching of the motor.

Highlights

The bacterial flagellum is a supramolecular machine essential for locomotion and virulence of many bacteria and comprises a long filament connected through a hook to a cell-enveloped embedded basal body.

The basal body comprises a bi-directional rotary motor energized by the stator units that surround it; the stator unit harnesses the electrochemical gradient of ions across the cytoplasmic membrane to generate torque.

Cryo-electron microscopic (cryo-EM) structures of the stator unit revealed its stoichiometry (a MotA pentamer surrounding a MotB dimer), its autoinhibition mechanism, the ion flux pathway, and the conformational changes upon protonation driving MotA rotation.

Phosphorylated chemotaxis signaling protein CheY-P binds to the C-ring of the flagellar motor, inducing a conformational change that alters the interaction between C-ring and stator units, switching the rotational direction of the flagellar motor from counterclockwise to clockwise.

The bacterial flagellum and its rotary motor

Many bacteria, including *Escherichia coli*, *Salmonella*, and *Bacillus* spp., use **flagella** (see Glossary) to move through liquid environments and across surfaces. The flagellum is a supramolecular nanomachine that protrudes from the cell envelope and measures ~5–20 μm in length. It is able to rotate in both **clockwise (CW) and counterclockwise (CCW)** directions to propel the bacterial cell body in different living environments [1,2]. Rotational switching between these two modes is regulated by **chemotactic signaling**, which is a rapid process that responds to environmental stimuli and biases movement of the cell toward attractants and away from repellents. Flagella-mediated chemotaxis further enables pathogenic bacteria to move toward cells to establish *in vivo* niches. [3,4]. Thus, flagella have fundamental roles in bacterial locomotion and virulence [5].

The flagellum comprises more than 25 kinds of building blocks, which assemble in a highly ordered manner. The flagellar structure can be divided into three morphologically distinguishable parts: a cell envelope-spanning motor (basal body), a universal joint (hook), and a long, thin helical filament [6,7] (Figure 1). Among them, the most intricate part is the basal body, containing the components responsible for assembly of the flagellum [the flagellar-specific **type-III secretion system** (T3SS) [8]], torque generation (the stator units [9]), and rotational switching (binding of the response regulator **CheY-P** to the cytoplasmic C-ring [10,11]). Cryo-ET studies of the motor from different bacterial species show the variation of its structure, while the core components are conserved [7,12,13]. For example, in the Gram-negative bacteria *Salmonella* and *E. coli*, the flagellar motor contains four ring-like structures based on their distributions relative to the cell surface layers [lipopolysaccharide (L-)ring, peptidoglycan (P-)ring, inner membrane/supramembrane (MS-)ring, and cytoplasmic (C-)ring] surrounding a central rigid rod [14–17]. Additional ring-like structures, H- and T-rings, located in the periplasmic space, have also been observed in *Vibrio* spp [18]. It is believed that assembly of the flagellar basal body initiates with formation of the core secretion pore FliPQR [19,20] of the flagellar-specific T3SS [21,22]. This

[1]Structural Biology of Molecular Machines Group, Protein Structure & Function Program, Novo Nordisk Foundation Center for Protein Research, Faculty of Health and Medical Sciences, University of Copenhagen, Blegdamsvej 3B, 2200 Copenhagen, Denmark
[2]Department of Molecular and Cellular Biology, Harvard University, 16 Divinity Avenue, Cambridge, MA 02138, USA
[3]Rowland Institute at Harvard, Harvard University, 100 Edwin H. Land Blvd, Cambridge, MA 02142, USA

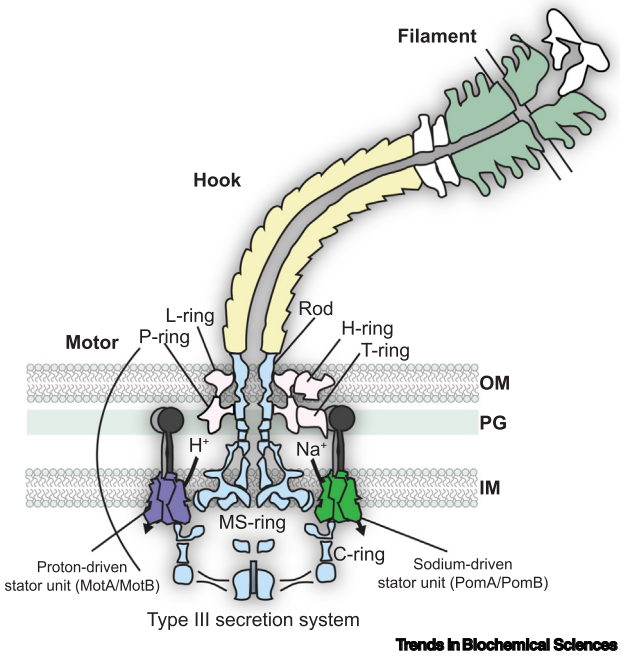

Figure 1. The architecture of the flagellum of Gram-negative bacteria. The left side corresponds to the motor with the H^+-dependent stator unit (MotA/MotB) and the right side shows the motor with the Na^+-dependent stator unit (PomA/PomB). The flagellar motor of marine *Vibrio* spp contains two additional ring structures: the T-ring and H-ring. Abbreviations: C-ring, cytoplasmic ring; IM, inner membrane; L-ring, lipopolysaccharide ring; MS-ring, inner membrane/supramembrane ring; OM, outer membrane; P-ring, peptidoglycan ring; PG, peptidoglycan.

[4]Institut für Biologie/ Bakterienphysiologie, Humboldt-Universität zu Berlin, Philippstr. 13, 10115 Berlin, Germany

*Correspondence: nicholas.taylor@cpr.ku.dk (N.M.I. Taylor).

is followed by subsequent assembly of the switch protein FlhB [23] and nine copies of the transmembrane protein FlhA [24], which is thought to couple energy derived from the proton-motive force to substrate protein secretion [25,26]. The MS-ring, which comprises multiple copies of the transmembrane protein FliF [17,27], forms a structural scaffold around the flagellar export apparatus and coordinates the formation of the C-ring, which engages with the stator units to generate torque [28].

The stator unit is a complex of two membrane proteins sharing the same operon on the genomic locus, with a molecular mass of ~200 kDa [29]. Located at the inner membrane, the stator unit is responsible for harvesting the cross-membrane electrochemical gradient of ions, most commonly protons or sodium ions (e.g., MotA/MotB is a H^+-dependent stator unit; PomA/PomB is a Na^+-dependent stator unit), while, in some cases, the stator unit also uses potassium and rubidium ions [30]. Some bacterial species contain only one type of stator unit, whereas others have multiple types [31]. For example, *Vibrio alginolyticus* contains only sodium-driven stator units and *Campylobacter jejuni* contains only proton-driven stator units, while *Bacillus subtilis* has both types [32]. In all stator units, one component is anchored to the bacterial cell wall, while the other component engages with the C-ring of the flagellar motor, thereby enabling torque generation.

The stator unit is considered as a motor itself: it converts the electrochemical potential energy from the ion motive force into mechanical torque. Upon recruitment to the basal body and cell wall binding, the stator units undergo a conformational change from an inactive/plugged state into an activated/unplugged state [33]. In the unplugged state, the flux of ions through the stator unit channel energizes the rotation of the rotor. Cryo-EM structures of stator units from different bacterial species have recently been determined to high resolution and their interactions with their rotors have been explored by cryo-tomographic studies [34–38]. Here, we focus on recent

developments in the understanding of the flagellar stator unit, the biological mechanism of its torque generation, and the rotational switching of the motor.

Structure of the stator unit

The C-terminal part of MotB or PomB [known as the peptidoglycan-binding (PGB) domain] allows binding of the stator unit to the peptidoglycan layer of the bacterial cell wall. The PGB domain displays a high degree of similarity to the C-terminal domain of OmpA, a flexible clamp responsible for bacterial cell wall binding [39]. High-resolution structures of isolated MotB PGB obtained through X-ray crystallography provide a wealth of information for a mechanistic understanding of its self-dimerization and its interaction with peptidoglycan components [40–42]. The intrinsic dynamic properties of the stator unit probably precluded crystallization of the full complex. The first available 3D structure of a stator unit was that of PomAB from *V. alginolyticus*, reconstructed by single-particle analysis from negatively stained samples, with a resolution limited to ~20 Å [43]. The map revealed the overall shape of the stator unit, suggesting that two PomB molecules were surrounded by four PomA monomers, consistent with previous studies establishing the presence of at least two PomB and an apparent PomA:PomB ratio of ~2:1 [44,45]. This model was widely used as template for molecular dynamic simulations of ion transportation and amino acid point mutagenesis for functional studies [43,46–48]. However, due to the low resolution of the structure, it was not possible to accurately interpret the stator unit stoichiometry and channel formation.

With the resolution revolution of single-particle cryo-EM, it became possible to determine high-resolution structures of membrane proteins without crystallization and with a smaller quantity of protein sample [49,50]. Both the relatively small molecular mass of the flagellar stator units as well as the preferred orientation that these particles adopt on EM grids have hindered their structural determination. By optimizing protein purification procedures and cryo-EM grid preparation, atomic models of the proton-driven MotAB stator unit family from three bacterial species were constructed [34,35]. These studies have contributed detailed structural information about the subunit assembly and proposed a mechanism for stator unit activation and torque generation.

The structures revealed that the stator unit adopts a $MotA_5$:$MotB_2$ arrangement. The 5:2 stoichiometry was also reinforced by low-resolution maps of two sodium-driven stator units, *V. alginolyticus* PomAB and *Vibrio mimicus* PomAB, albeit lacking the atomic coordinates [34,35]. These data suggest a conserved arrangement across all types of flagellar stator unit: a pentamer of MotA peripherally surrounding a dimer of MotB (Figure 2A,C). Of note, all three models lack the MotB C-terminal PGB domain, reflecting the highly flexible locations of MotB PGB with respect to the core structure, at least in a detergent environment [34,35]. Moreover, the structures suggest that the stator unit is in an autoinhibited state (discussed later). Other evolutionarily related bacterial complexes, which also harness the transmembrane proton motive force, share the same 5:2 stoichiometry [51,52]. These include $ExbB_5D_2$, which powers the ExbB–ExbD–TonB complex, responsible for transportation of nutrients entering into the periplasmic space [53], and $GldL_5M_2$, which powers the gliding motility/type 9 protein secretion system motors in members of the phylum *Bacteroidetes* [54].

Among the different stator units studied, the structure of MotAB has been determined from *C. jejuni* (*Cj*MotAB), a common foodborne pathogenic bacterium [55], to a resolution of 3.1 Å (with a local resolution as high as 2.5 Å) [34]. Briefly, the transmembrane segments (TM) of MotA fold into α helices, with the third and fourth segments (TM3 and TM4) lining the dimerized MotB TM helices. MotA TM1 and TM2 establish extensive hydrophobic interactions with the lipid bilayer. Two amphipathic helices of MotA, the cytoplasmic interface helix (CI) and the

Glossary

Bis-(3′-5′)-cyclic dimeric guanosine monophosphate (c-di-GMP): also called cyclic diguanylate or cyclic-di-GMP; a global bacterial second messenger molecule involved in signal transduction of a range of cellular processes.
Chemotactic signaling: rapid process that responds to environmental stimuli and biases movement of the cell toward nutrients and away from repellents.
CheY-P: a phosphorylated form of a response regulator protein that can bind to the flagellar motor to alter the rotational direction of the motor.
Clockwise (CW) and counterclockwise (CCW) directions: flagella are able to rotate in both CW (viewed from filament to motor) and CCW directions to propel the bacterial cell body in different liquid environments. Cells of peritrichously flagellated *Escherichia coli* and *Salmonella* move forward when their flagella rotate CCW (when a flagellar bundle forms) and tumble when the rotation direction switches to CW (which causes the flagellar bundle to fall apart).
Flagellum: proteinaceous motility device embedded in the cell envelope of many bacteria. The bacterial flagellum enables bacteria to swim in liquid environments or swarm on solid surfaces.
Periplasmic flagella: some bacteria, such as *Spirochetes*, have flagella that reside within the periplasmic space.
Peritrichously flagellated bacterium: a bacterial cell that has several flagella distributed randomly on its cell body.
Single polar flagellum: bacterium that has only one flagellum that attaches to its cell pole.
***Trans* mode:** indicates that the two plug motifs from two MotB chains are on the opposing sides of the two MotB transmembrane helices.
Type-III secretion system (T3SS): a protein secretion system found at the base of the bacterial flagellum and of the needle-like injectisome. The injectisome is a major virulence factor of many Gram-negative bacteria and responsible for injection of proteins directly from the bacterial cell into the eukaryotic host cell.

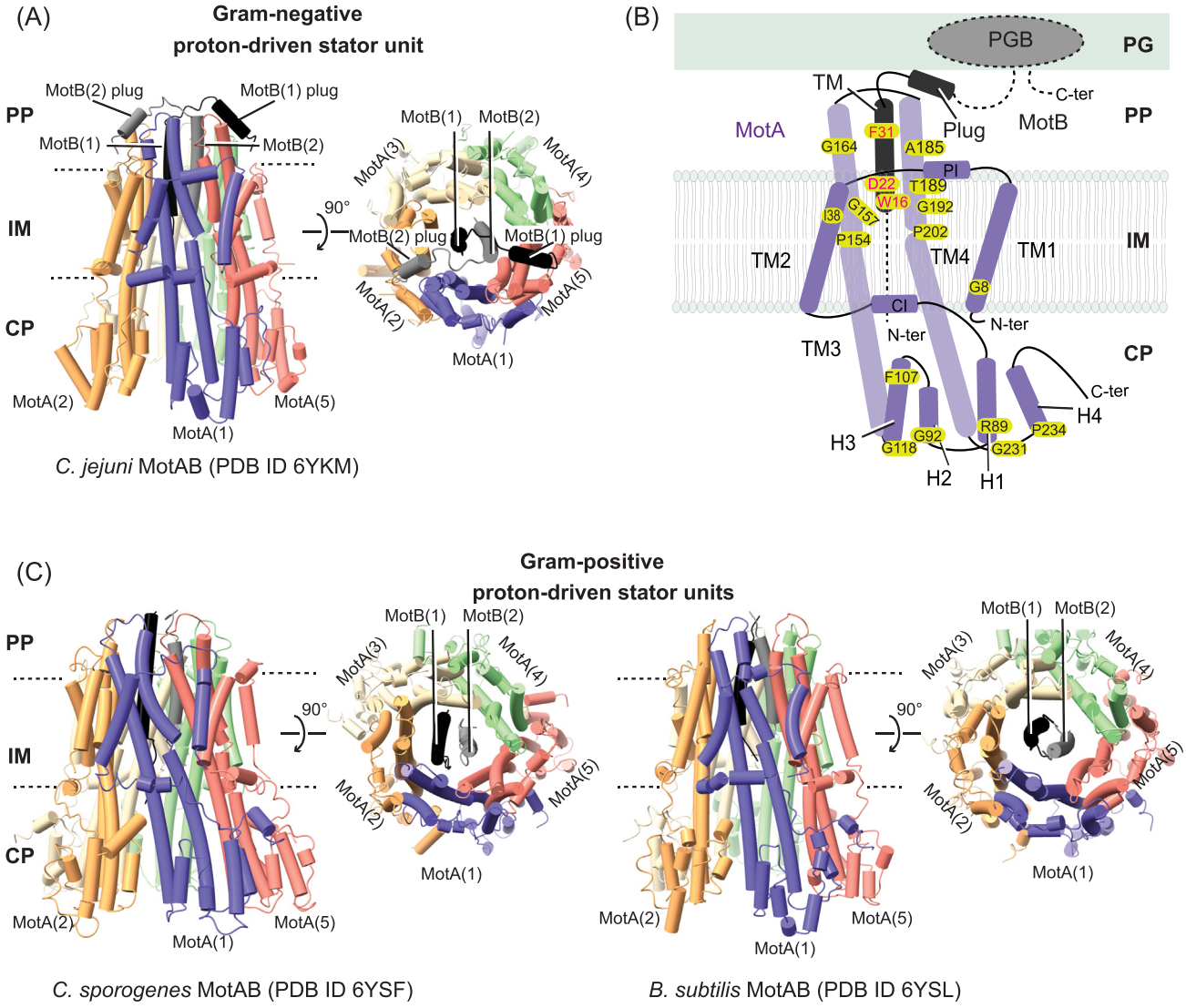

Figure 2. Available atomic structures of flagellar stator units. (A) Proton-driven MotAB from the Gram-negative bacterium *Campylobacter jejuni* (*Cj*MotAB) [Protein Data Bank (PDB) ID: 6YKM]. Subunits are present in a $MotA_5$:$MotB_2$ stoichiometry. MotA subunits (purple, orange, yellow, green, and red) surround MotB subunits (black and gray). MotB plug motifs are shown in the periplasmic space. (B) Topology organization and secondary structural elements of *Cj*MotA (purple) and *Cj*MotB (black) subunits. The OmpA-like MotB peptidoglycan-binding domain (PGB) is indicated as a gray ellipse. The strictly conserved residues among stator units from different bacterial species are shown as yellow ovals, with red text for conserved residues belonging to MotB and black for MotA. (C) Left: proton-driven MotAB from the Gram-positive bacterium *Clostridium sporogenes* (PDB ID: 6YSE). Right: proton-driven MotAB from the Gram-positive bacterium *Bacillus subtilis* (PDB ID: 6YSL). Structures are colored as in (A). In this case, the plug motifs are not built in both original models due to the local map quality. Abbreviations: CI, cytoplasmic interface; CP, cytoplasm; H, helix; IM, inner membrane; PI, periplasmic interface; PG, peptidoglycan; PP, periplasm; TM, transmembrane.

periplasmic interface helix (PI), perpendicular to the TM3 and TM4, adopt a parallel orientation with reference to the membrane, clearly defining the membrane boundary of the stator unit (Figure 2A,B); this is consistent with the structures of the MotAB stator units from *B. subtilis* and *Clostridium sporogenes* [34,35]. At the periplasmic interface, a short helix just after the TM of MotB, designated as a plug motif, wedges in between the top of two MotA subunits, revealing the autoinhibition mechanism of the stator unit [34] (Figure 2B). The plug motifs of the two MotB chains are organized in a ***trans* mode** in the stator unit, consistent with earlier functional

experiments [33] (Figure 3A). The density around the first ten residues of the MotB N terminus is less defined, preventing model building, suggesting that this region adopts different conformations [34,35]. Additionally, the unplugged structure of *Cj*MotAB (MotB 41–60) mimicking the active state of the stator unit, and the unplugged and protonated structure of *Cj*MotAB (MotB 41–60, D22N)

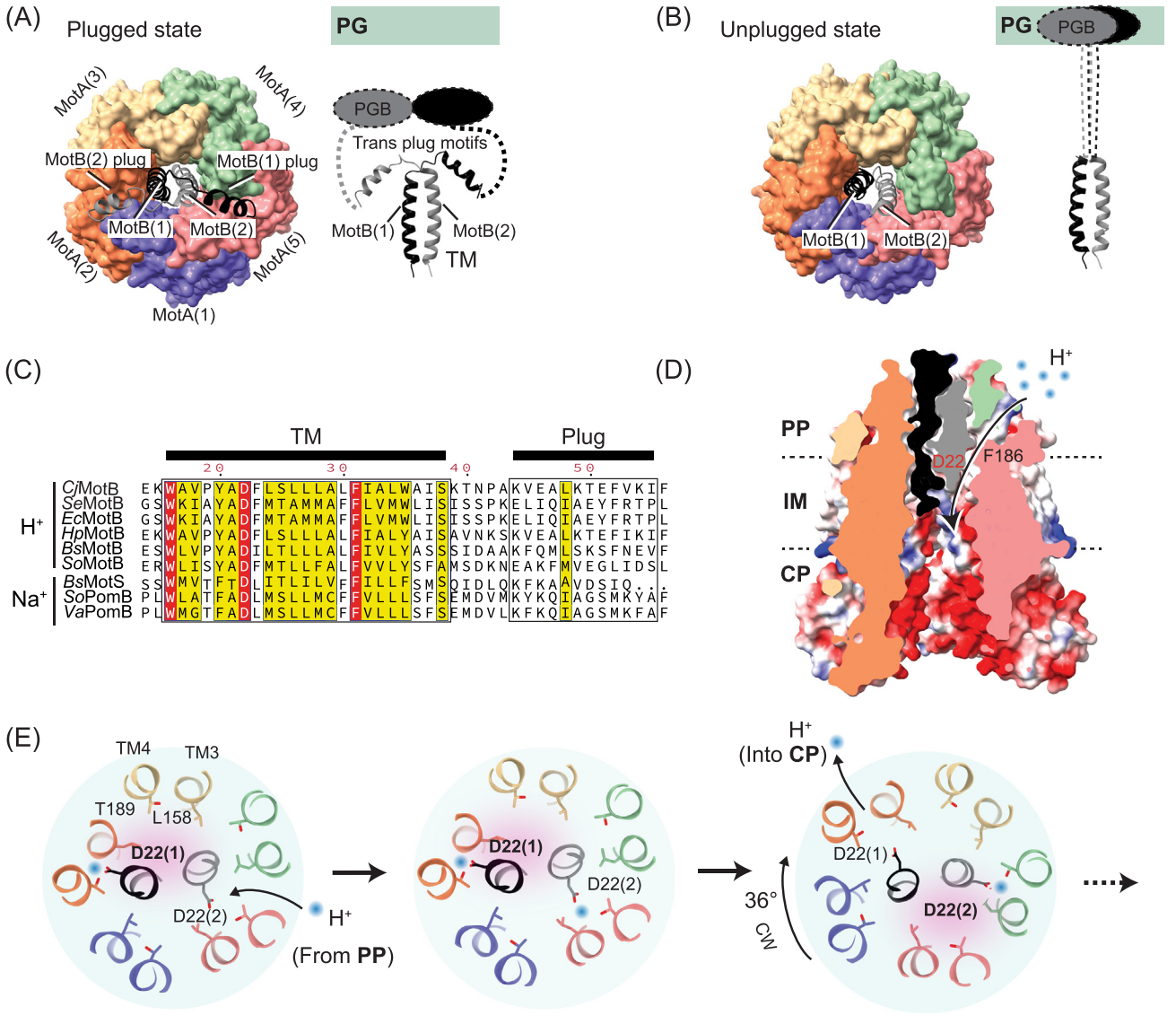

Figure 3. Activation and rotation mechanisms of the *Campylobacter jejuni* (Cj)MotAB stator unit. (A) Left: top view of *Cj*MotAB stator unit in its autoinhibited state with MotB shown as a cartoon representation and MotA shown as a surface representation [Protein Data Bank (PDB) ID: 6YKM]. Right: organization of MotB transmembrane helix and plug motif. MotB plug motifs function in *trans* mode. Colored as in Figure 2A in the main text. (B) Left: top view of *Cj*MotAB stator unit in its unplugged state (PDB ID: 6YKP). Right: activation of the stator unit requires the dimerized MotB PGB to bind to the peptidoglycan (PG) layer, unplugging the channel. (C) Multiple-sequence alignment of *Cj*MotB transmembrane (TM) helix and plug motif with different proton- and sodium-dependent homologs to highlight the conserved residues. (D) View from within the membrane showing the potential proton channel of the *Cj*MotAB stator unit in the unplugged conformation. (E) Mechanistic model for proton motive force-powered rotation of MotA around MotB. D22 from MotB engaged with MotA is highlighted with pink halos. Left: MotB chain 1 D22 [D22(1)] is coupled with a proton or hydronium and MotB chain 2 D22 [D22(2)] receives a proton or hydronium from the periplasmic (PP) side. Middle: proton or hydronium binding neutralizes MotB D22(2) charge. Right: MotA rotates 36° clockwise (CW) by a power stroke. MotB D22(1) releases the proton or hydronium into the cytoplasm (CP) and MotB D22(2) (charge is neutralized) gets in a position similar to the MotB D22(1) in the left panel.

were characterized to a high resolution [34] (Figure 3B). Given that the architecture and the sequence of the stator units are so well conserved, these high-resolution structures offer a great opportunity to understand how ions flow through the stator unit and induce rotation of MotA around MotB.

Stator unit activation, ion flux pathway, and rotation

One distinctive, universally conserved feature in MotB is the plug motif. Early functional experiments showed that overexpression of MotAB from *E. coli* did not impair cell growth [56]. By contrast, in-frame deletion of this plug motif leads to proton leakage and cell growth arrest, showing that activation of the MotAB channel is controlled by the plug motif [33,57]. As noted earlier, the structure of the unplugged state of *Cj*MotAB was obtained by deleting the residues corresponding to the plug motif [34]. Interestingly, it was observed that the unplugged *Cj*MotAB was toxic to *E. coli* cells when overexpressed [34].

This unplugged structure unveils a potential proton channel that links the periplasmic space to the conserved acidic residue D22 on TM helix of MotB chain 2 (Figure 3D) (numbering to reflect the specific local environment of each segment in the asymmetric complex), and to the inside of MotA cytoplasmic domain, where many negatively charged residues are found [34]. Inspection of the channel-lining residues reveals the differential conservation between proton and sodium-dependent stator units, which have previously been shown to be critical for ion transport (Figure 3C) [58–60]. In addition, this channel is shielded by the conserved hydrophobic residue F186 of TM4 of MotA, the side chain of which adopts two different conformations [34]. Consequently, this residue is likely to be a key point controlling the ion flux, ensuring efficient ion motive force utilization. D22 on the TM of *Cj*MotB chain 1 is buried in a hydrophobic environment; therefore, it is more likely to accommodate a protonated (or hydronium-interacting) D22 compared with the MotB chain 2 [34]. Supporting this model, the proton channel is not observed in any of the three plugged stator units [34,35].

The comparison between plugged and unplugged MotAB structures reveals no major conformational differences, which argues against the idea that a large conformational change within MotA, without rotation of MotA around MotB, causes torque generation, which was the previous paradigm [61]. Rather, it strongly suggests a rotational mechanism [34,35]. In the active state of the stator unit, the PGB domains of the two MotB chains are dimerized and anchored to the peptidoglycan layer; therefore, only MotA can rotate around MotB [35] (Figure 3B). Based on this structural analysis [34], it was hypothesized that MotB chain 1 D22 is bound to a proton or hydronium ion and engaged to MotA. It is ready to perform a power stroke, but rotation is blocked because the negatively charged MotB chain 2 D22 cannot move across the hydrophobic surface of the stator unit. Then, MotB chain 2 D22 receives a proton or a hydronium ion from the periplasmic side, now allowing MotA to rotate. This is because this neutralized, disengaged MotB chain 2 D22 can now enter a hydrophobic region, such as the MotB chain 1 D22, where it must be deprotonated to release the bound proton or hydronium into the cytoplasm. Indeed, structural comparison between the unplugged and D22N unplugged mutants revealed how D22 changes from pointing to the periplasm in the deprotonated state to pointing down toward the cytoplasmic interface when protonated [34]. After MotB chain 1 D22 has released its proton, MotB chains 1 and 2 have now functionally switched roles and the cycle can start again. Consequently, each proton transport event triggers MotA rotation around MotB by 36° in a clockwise direction (Figure 3E). This is reminiscent of the mechanism that an inchworm uses for locomotion (or to the working mechanism of human-made inchworm motors) [34,62]. The cytoplasmic lumen of MotA could serve as an electrostatic complementarity reservoir, attracting and housing the incoming ions. Collectively, the structural features of the stator unit in both plugged and unplugged

states explain how MotA rotates around MotB upon stator unit activation and ion motive force dispersion.

Another alternative, which still implies a rotational model, has been proposed by Deme *et al.*, in which MotA would also rotate 36° around MotB for every ion-binding/release event, but in which only one of the two MotB chains would be protonated simultaneously [35]. This model is similar to that suggested by Santiveri *et al.*, but the difference is that, in the latter, both MotB chains would need to be protonated simultaneously to trigger the power stroke [34]. We suggest that this model is the most likely because the hydrophobic MotA interior would likely only be able to rotate around MotB when the latter is charge neutralized.

Additionally, Deme *et al.* proposed a second rotational model in which MotA rotates 36° around MotB and then resets to the original position [35]. This alternative is less likely because this mechanism requires that the stator unit detaches from the rotor, and this is not in line with the observed high duty ratio of the motor [63]. By contrast, the implied handover mechanisms in the unidirectional rotational models would allow the rotor and stator to remain firmly associated all the time and are consistent with a high duty ratio.

An atomic model of a sodium-driven stator unit is still lacking; therefore, it remains unclear how the stator unit recognizes the coupling sodium ion. The two types of stator unit share a similar architecture, and the universally conserved aspartate residue involved in ion binding is located at a similar level of the MotB TM helix [64]. A recent study with *Bacillus clausii*, an alkaliphilic bacterium, showed that its stator unit can use both Na^+ and H^+ as coupling ions, depending on the environmental pH [65]. Different triple mutations of residues at the periplasmic side of MotB TM switched the dual-functional stator unit into either a proton-driven or sodium-driven one, indicating that ion specificity is located along the channel at the region preceding the critically conserved aspartate [65]. Introduction of sodium-driven PomAB into *E. coli* through CRISPR/Cas-mediated genome engineering showed that, when sodium is lacking, PomAB can spontaneously mutate, which allows it to use the proton gradient as driving force [66]. Thus, additional studies are needed to fully understand the molecular basis underlying the ion selectivity mechanism of the stator unit.

Interaction between the stator unit and rotor

The C-ring forms a cup-like structure located at the cytoplasmic base of the flagellar rotor, and is essential for torque generation and flagellar rotation [13,67]. Cryo-ET studies of the flagellar motor revealed the overall architecture and general shape of the C-ring [15]. For example, in *E. coli* and *Salmonella*, the C-comprises a complex of three proteins: FliG, FliM, and FliN (Figure 4A). Other bacterial species, such as *B. subtilis*, *Thermotoga maritima*, and *Listeria monocytogenes*, additionally contain FliY as a supplementary subunit to, or instead of, FliN [68–70].

Several crystal structures of different C-ring proteins and subcomplexes, as well as crosslinking experiments, provide important information regarding protein–protein interactions and C-ring assembly. X-ray structures of isolated domains of FliG [71,72] and the full-length protein from the thermophile *Aquifex aeolicus* have been determined [73]. FliG comprises three domains: an N-terminal domain ($FliG_N$), responsible for binding to the MS-ring; a C-terminal domain ($FliG_C$), containing a torque helix that interacts with the stator units [73]; and a middle domain ($FliG_M$), providing the binding site for FliM. The crystal structure of the cytoplasmic domain of FliF ($FliF_C$) in complex with $FliG_N$ from *Helicobacter pylori* revealed the assembling interface between the C-ring and MS ring [74]. This interaction allows attachment of the C-ring close to the inner membrane and is important for its assembly [74]. Recent cryo-EM analysis reported high-resolution

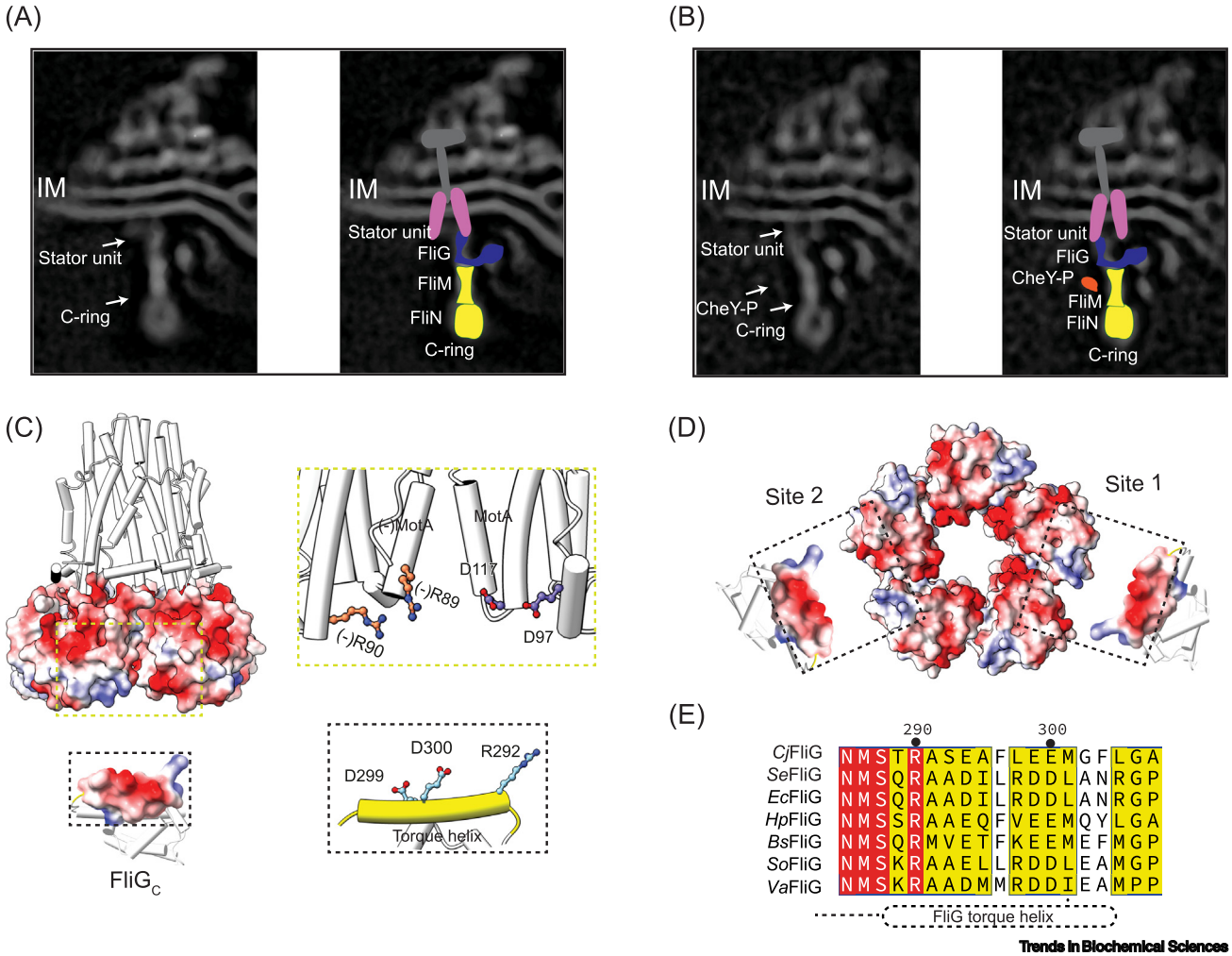

Figure 4. Interactions between stator unit and rotor. (A) A section from a tomogram of a *Borrelia burgdorferi* flagellar motor *in situ* (EMD-21886) showing the direct interactions between the stator unit and the C-ring. (B) The C-ring undergoes a conformational change and interacts with the different sides of the stator unit (EMD-21884). (C) Left: the calculated electrostatic potential (negatively charged, red; positively charged, blue) of the *Campylobacter jejuni* (Cj)MotA cytoplasmic domain (based on the built atomic model) and the *Cj*FliG C-terminal domain (based on homology modeling) that contains the torque-generating helix. Right: charged residues, shown in stick representation, on the potential interaction interface between the cytoplasmic domain of *Cj*MotA and the torque helix of *CjFliG*. (D) The potential two interactions interfaces between the stator unit and the C-ring. In counterclockwise (CCW) rotation of the motor, the FliG torque helix interacts with the inside cytoplasmic surface of the stator unit (the side proximal to the motor axis). In clockwise (CW) rotation of the motor, the FliG torque helix flips 180° and interacts with the outside surface of the stator unit. (E) Multiple-sequence alignment of the torque-generating helix of the FliG C-terminal domain from different bacterial species to highlight the conserved charged residues.

structures of the MS-ring from *Salmonella typhimurium*, both from purified FliF and from the native motor, unveiling that the MS-ring adopts a 34-fold symmetry [17,27,75]. Furthermore, directed point mutagenesis and crosslinking experiments showed a 1:1 stoichiometric interaction between FliG and FliF, indicating that the C-ring also contains 34 FliG protomers [76,77]. FliM also comprises three domains [78]. The N-terminal domain of FliM ($FliM_N$) contains the binding site for the phosphorylated chemotaxis signaling protein CheY (CheY-P). The middle domain of FliM ($FliM_M$) binds to $FliG_M$ [79]. The C-terminal domain ($FliM_C$) dimerizes with FliN [80], which locates at the bottom of the C-ring.

From the combined insights of the full-length structure of FliG and tomographic studies, it was inferred that FliG multimers undergo a dramatic conformational change during the flagellar

motor switching between the CCW and CW rotational direction. In the CCW rotational mode, FliG adopts a closed, compact form (Figure 4A), whereas, in the CW rotational mode, it adopts an extended and open form [73] (Figure 4B). The conformational change of FliG during directional switching was confirmed by recent cryo-ET studies [38], in which the authors showed the unique composition and dynamic features of the C-ring that control motor rotational switching by changing the interaction interface between stator unit and rotor.

The electrostatic interactions between stator units and rotor are essential for torque generation [81–83]. Sequence comparison reveals conserved charged residues located in the large cytoplasmic domain of MotA, which is proposed to be its interaction interface with $FliG_N$ [34]. In *E. coli* and *Salmonella enterica*, chromosomal point mutations of these residues to alanine or to amino acids with the opposite charge decrease or completely abolish bacterial motility, showing that this electrostatic interaction contributes to torque generation and the proper assembly of the stator unit around the rotor [84]. Similar phenomena were also observed in *V. alginolyticus*, in which the stator units harness the inner membrane sodium gradient to drive rotation of the motor [85,86]. In *Cj*MotAB, the FliG torque helix-binding site is most likely located at the cleft between two MotA subunits, involving the positively charged residues R89 and R90 from one MotA subunit and the negatively charged residues D97 and D117 from the adjacent subunit [34] (Figure 4C). During MotA rotation around MotB, at least one of these binding sites incorporates the FliG torque helix through interactions by reversed charged residues (Figure 4D). Multiple-sequence alignment of the torque-generating helix of the $FliG_C$ showed that these charged residues are conserved among different bacterial species (Figure 4E). In addition, cryo-ET and subtomogram averaging enabled visualization of the interaction *in situ*, supporting the direct interplay between stator units and C-ring proteins FliG [36] (Figure 4A,B).

The number of stator units assembled around the rotor is variable. In some flagellar motors, the stator units are constantly exchanged with those in the membrane pool [87,88] in a load-dependent manner [89,90]. An increase in load promotes assembly of stator units, while a reduction promotes disassembly [91,92]. This mechanosensitive turnover is driven by a catch bond, a type of interaction that becomes stronger instead of weaker under force [91]. Recent work showed that this load-dependent remodeling is independent of the direction of rotation of the motor, suggesting a passive mechanical mechanism [93]. Such dynamic remodeling of the stator unit enables the flagellar motor to efficiently adapt its output to changes in the external load.

Mechanism of bi-directional rotation of the flagellar motor

In **peritrichously flagellated bacteria**, the external flagella are able to rotate in both CW and CCW directions. Cells move forward when their flagella rotate CCW and tumble when the rotation switches to CW [7,94]. Although this is the case for *E. coli* and *Salmonella*, other flagellated bacteria swim differently. For instance, *V. alginolyticus* has a **single polar flagellum** that pushes (CCW rotation) or pulls (CW rotation) the cell body [95]. Another example is that of spiral-shaped bacteria, also called spirochetes, which contain **periplasmic flagella** that lie in between the inner and outer membranes. This unique feature makes spiral-shaped bacterial motility different from that of most other motile bacteria. When the flagella at one cell pole rotate in CCW direction and the flagella at the other cell pole rotate CW, the cell moves forward. When the flagella at both poles rotate in the same direction, the cell flexes in place [38,96]. An additional interesting phenomenon that illustrates the variety in swimming mechanisms of flagellated bacteria is found in *Sinorhizobium meliloti* and *Rhodobacter sphaeroides* the flagella of which rotate only CW; these bacteria reorient themselves through Brownian motion upon slowing down and upon stopping rotation, respectively [97,98].

In flagellar motors that rotate in both CW and CCW directions, the structural features of the stator unit combined with the assumption of its unidirectional CW rotation upon ion permeation lead to a model of the rotational directionality of the flagellar motor [34,99]. In CCW rotation of the motor, the FliG torque helix interacts with the inside cytoplasmic surface of the stator unit (the side proximal to the motor axis) (Figure 5A). CW rotation of the motor is achieved by remodeling of the C-ring through a conformational change of FliG upon chemotaxis signaling: the FliG torque

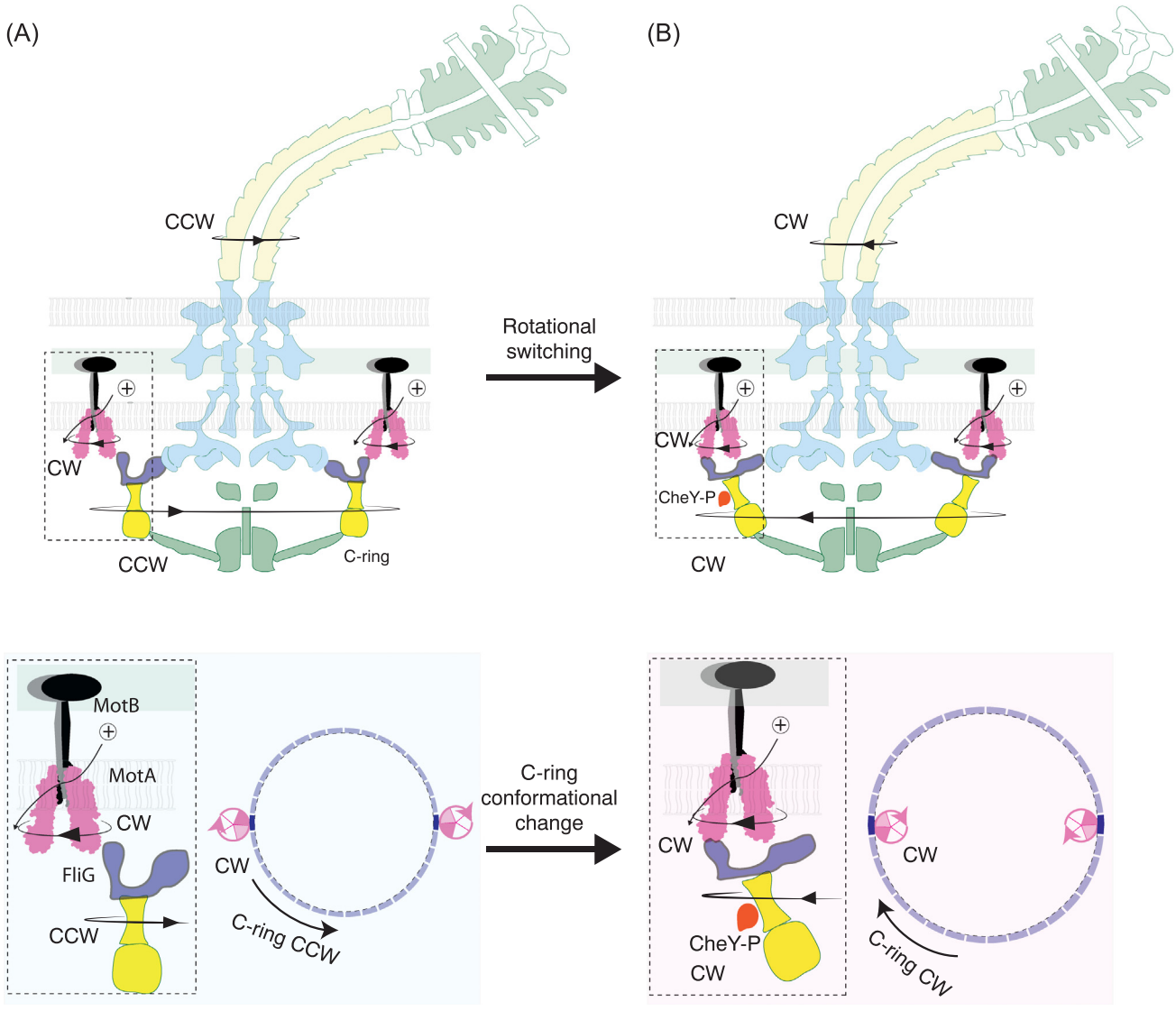

Figure 5. Mechanistic model of rotational switching. (A) Top: interactions of the unplugged stator unit (MotA, pink; MotB, black) with the C-ring (purple, yellow, and green) during counterclockwise (CCW) rotation. The influx of protons drives the stator unit to rotate in a clockwise (CW) mode. When phosphorylated, CheY-P is not bound, and the torque helix of FliG (purple) interacts with the inside cytoplasmic surface of the stator unit (the side proximal to the motor axis), causing the C-ring to rotate in a CCW mode. Bottom: schematic of the rotor–stator unit scale, symmetry, and interaction. The expected FliG stoichiometry (34-fold; purple) is represented by splitting up the disc ring in 34 equally sized slices. The fivefold stoichiometry and pseudo-symmetry of MotA (pink) is represented. (B) Top: interaction of the stator unit with the C-ring during CW rotation. When the phosphorylated (i.e., activated), CheY-P (red) binds to the C-ring, FliG (purple) undergoes a conformational change, and the torque helix now interacts with the outside cytoplasmic surface of the stator unit (the side facing away from the motor axis), causing the C-ring to rotate in a CW mode. Bottom: schematic of the rotor–stator unit scale, symmetry, and interaction during CW rotation of the C-ring, showing that FliG adopts an extended and open form in this CW rotational mode.

helix turns 180° around the stator unit, allowing it to now interact with the outside surface of the stator unit [34,35,38] (Figure 5B). The FliG conformational change is the final step in a sophisticated chemotaxis signaling system that allows the bacterium to sense chemical stimuli and transmit this information through the phosphorylated form of the response regulator protein, CheY [100]. Binding of CheY-P to FliM changes the direction of the flagellar motor rotation by inducing a concerted conformational change of the C-ring, causing switching from CCW to CW [101]. This model is supported by an observation in an *E. coli* strain lacking the gene encoding CheY, in which flagellar rotation is locked in the CCW direction [10,11]. Cryo-ET studies of *Borrelia burgdorferi* [38] and *V. alginolyticus* [37] revealed *in situ* the conformational change of the C-ring during rotational switching, in which FliG is present in different orientations in relation to the stator unit.

Concluding remarks

The flagellar stator unit, which powers bi-directional rotation of the flagellum, is one of the smallest motors found in bacteria. The recent cryo-EM structures of the flagellar stator units of different bacterial species in their autoinhibited and unplugged states, together with biochemical studies, revealed the architecture of the stator unit as well as its rotation mechanism upon ion permeation [34,35]. These high-resolution structures also reveal the ion translocation pathway. Together with recent cryo-ET data [36–38], they also suggest a plausible model for torque generation and switching of the rotational direction of the flagellar motor.

Yet, many questions still remain (see Outstanding questions). For example, how does the stator unit select different types of ion? This will require determining a high-resolution structure of the sodium-driven stator unit, ideally in its different functional states. Several sodium channel blockers, including amiloride and its analogs, such as phenamil, specifically inhibit the sodium-driven stator unit, although their inhibition mechanism remains to be revealed at the molecular level [102]. Furthermore, the binding interface of the stator unit and flagellar rotor (MotA-FliG and PomA-FliG) is blocked by YcgR, which acts as a flagellar brake protein in a manner that depends on the second messenger **bis-(3′-5′)-cyclic dimeric guanosine monophosphate (**c-di-GMP) [103,104]. What is the structural basis underlying this ‘brake’ mechanism? It is clear such questions will benefit from high-resolution structures of the entire flagellar motor encompassing the stator units and the C-ring, which are yet to be obtained. Furthermore, if the proposed torque generation model can be validated in living bacterial cells, it can become clear whether and how stator unit action is coupled with torque generation. It is an exciting time for research on the bacterial flagellar motor, and the next few years will undoubtedly reveal many more of its secrets.

Outstanding questions

What is the atomic structure of the sodium-driven stator unit and how does it explain the molecular mechanism of coupling ion selectivity of the stator unit?

What is the structural basis underlying the ‘brake’ mechanism triggered by YcgR?

What are the conformational changes of FliG upon CheY-P binding to the C-ring?

How does the stator unit couple with the different conformational states of the FliG to generate torque?

Can the proposed torque generation model be validated in living bacterial cells?

Acknowledgments

The Novo Nordisk Foundation Center for Protein Research is supported financially by the Novo Nordisk Foundation (NNF14CC0001). N.M.I.T. acknowledges support from a DFF grant (8123-00002B), NNF Hallas-Møller Emerging Investigator grant (NNF17OC0031006), and the EMBO Young Investigator programme. H.H. acknowledges support from the Lundbeck Foundation (postdoc grant R347-2020-2429). N.W. was supported by the National Institute of General Medical Sciences of the National Institutes of Health under Award Number K99GM134124.

Declaration of interests

None declared by authors.

References

1. Nakamura, S. and Minamino, T. (2019) Flagella-driven motility of bacteria. *Biomolecules* 9, 279
2. Armitage, J.P. and Berry, R.M. (2020) Assembly and dynamics of the bacterial flagellum. *Annu. Rev. Microbiol.* 74, 181–200
3. Rivera-Chávez, F. *et al.* (2013) *Salmonella* uses energy taxis to benefit from intestinal inflammation. *PLoS Pathog.* 9, e1003267
4. Horstmann, J.A. *et al.* (2020) Methylation of *Salmonella typhimurium* flagella promotes bacterial adhesion and host cell invasion. *Nat. Commun.* 11, 2013

5. Chaban, B. *et al.* (2015) The flagellum in bacterial pathogens: for motility and a whole lot more. *Semin. Cell Dev. Biol.* 46, 91–103
6. Berg, H.C. (2003) The rotary motor of bacterial flagella. *Annu. Rev. Biochem.* 72, 19–54
7. Carroll, B.L. and Liu, J. (2020) Structural conservation and adaptation of the bacterial flagella motor. *Biomolecules* 10, 1492
8. Halte, M. and Erhardt, M. (2021) Protein export via the Type III secretion system of the bacterial flagellum. *Biomolecules* 11, 186
9. Blair, D.F. and Berg, H.C. (1990) The MotA protein of *E. coli* is a proton-conducting component of the flagellar motor. *Cell* 60, 439–449
10. Alon, U. *et al.* (1998) Response regulator output in bacterial chemotaxis. *EMBO J.* 17, 4238–4248
11. Welch, M. *et al.* (1993) Phosphorylation-dependent binding of a signal molecule to the flagellar switch of bacteria. *Proc. Natl. Acad. Sci. U. S. A.* 90, 8787–8791
12. Beeby, M. *et al.* (2016) Diverse high-torque bacterial flagellar motors assemble wider stator rings using a conserved protein scaffold. *Proc. Natl. Acad. Sci. U. S. A.* 113, E1917–E1926
13. Kaplan, M. *et al.* (2019) The presence and absence of periplasmic rings in bacterial flagellar motors correlates with stator type. *eLife* 8, e43487
14. Oikonomou, C.M. *et al.* (2016) A new view into prokaryotic cell biology from electron cryotomography. *Nat. Rev. Microbiol.* 14, 205–220
15. Chen, S. *et al.* (2011) Structural diversity of bacterial flagellar motors. *EMBO J.* 30, 2972–2981
16. Tan, J. *et al.* (2021) Structural basis of assembly and torque transmission of the bacterial flagellar motor. *Cell* 184, 2665–2679
17. Johnson, S. *et al.* (2021) Molecular structure of the intact bacterial flagellar basal body. *Nat. Microbiol.* 6, 712–721
18. Zhu, S. *et al.* (2017) Molecular architecture of the sheathed polar flagellum in Vibrio alginolyticus. *Proc. Natl. Acad. Sci. U. S. A.* 114, 10966–10971
19. Johnson, S. *et al.* (2019) The structure of an injectisome export gate demonstrates conservation of architecture in the core export gate between flagellar and virulence Type III secretion systems. *mBio* 10, e00818-19
20. Kuhlen, L. *et al.* (2018) Structure of the core of the type III secretion system export apparatus. *Nat. Struct. Mol. Biol.* 25, 583–590
21. Fabiani, F.D. *et al.* (2017) A flagellum-specific chaperone facilitates assembly of the core type III export apparatus of the bacterial flagellum. *PLoS Biol.* 15, e2002267
22. Fukumura, T. *et al.* (2017) Assembly and stoichiometry of the core structure of the bacterial flagellar type III export gate complex. *PLoS Biol.* 15, e2002281
23. Kuhlen, L. *et al.* (2020) The substrate specificity switch FlhB assembles onto the export gate to regulate type three secretion. *Nat. Commun.* 11, 1296
24. Abrusci, P. *et al.* (2013) Architecture of the major component of the type III secretion system export apparatus. *Nat. Struct. Mol. Biol.* 20, 99–104
25. Erhardt, M. *et al.* (2017) Mechanism of type-III protein secretion: regulation of FlhA conformation by a functionally critical charged-residue cluster. *Mol. Microbiol.* 104, 234–249
26. Paul, K. *et al.* (2008) Energy source of flagellar type III secretion. *Nature* 451, 489–492
27. Kawamoto, A. *et al.* (2020) Native structure of flagellar MS ring is formed by 34 subunits with 23-fold and 11-fold subsymmetries. *bioRxiv* Published online October 11, 2020. https://doi.org/10.1101/2020.10.11.334888
28. Terashima, H. *et al.* (2020) Assembly mechanism of a supramolecular MS-ring complex to initiate bacterial flagellar biogenesis in *Vibrio* species. *J. Bacteriol.* Published online June 1, 2020. https://doi.org/10.1128/JB.00236-20
29. Liu, R. and Ochman, H. (2007) Origins of flagellar gene operons and secondary flagellar systems. *J. Bacteriol.* 189, 7098–7104
30. Terahara, N. *et al.* (2012) A *Bacillus* flagellar motor that can use both Na+ and K+ as a coupling ion is converted by a single mutation to use only Na+. *PLoS ONE* 7, e46248
31. Paulick, A. *et al.* (2015) Dual stator dynamics in the *Shewanella oneidensis* MR-1 flagellar motor. *Mol. Microbiol.* 96, 993–1001
32. Minamino, T. *et al.* (2018) Autonomous control mechanism of stator assembly in the bacterial flagellar motor in response to changes in the environment. *Mol. Microbiol.* 109, 723–734
33. Hosking, E.R. *et al.* (2006) The *Escherichia coli* MotAB proton channel unplugged. *J. Mol. Biol.* 364, 921–937
34. Santiveri, M. *et al.* (2020) Structure and function of stator units of the bacterial flagellar motor. *Cell* 183, 244–257
35. Deme, J.C. *et al.* (2020) Structures of the stator complex that drives rotation of the bacterial flagellum. *Nat. Microbiol.* 5, 1553–1564
36. Chang, Y. *et al.* (2019) Structural insights into flagellar stator–rotor interactions. *eLife* 8, e48979
37. Carroll, B.L. *et al.* (2020) The flagellar motor of *Vibrio alginolyticus* undergoes major structural remodeling during rotational switching. *eLife* 9, e61446
38. Chang, Y. *et al.* (2020) Molecular mechanism for rotational switching of the bacterial flagellar motor. *Nat. Struct. Mol. Biol.* 27, 1041–1047
39. Samsudin, F. *et al.* (2016) OmpA: a flexible clamp for bacterial cell wall attachment. *Structure* 24, 2227–2235
40. Roujeinikova, A. (2008) Crystal structure of the cell wall anchor domain of MotB, a stator component of the bacterial flagellar motor: Implications for peptidoglycan recognition. *Proc. Natl. Acad. Sci. U. S. A.* 105, 10348–10353
41. Zhu, S. *et al.* (2014) Conformational change in the periplamic region of the flagellar stator coupled with the assembly around the rotor. *Proc. Natl. Acad. Sci. U. S. A.* 111, 13523–13528
42. O'Neill, J. *et al.* (2011) Role of the MotB linker in the assembly and activation of the bacterial flagellar motor. *Acta Crystallogr. D Biol. Crystallogr.* 67, 1009–1016
43. Yonekura, K. *et al.* (2011) Structure of the flagellar motor protein complex PomAB: implications for the torque-generating conformation. *J. Bacteriol.* 193, 3863–3870
44. Sato, K. and Homma, M. (2000) Functional reconstitution of the Na+-driven polar flagellar motor component of *Vibrio alginolyticus*. *J. Biol. Chem.* 275, 5718–5722
45. Braun, T.F. and Blair, D.F. (2001) Targeted disulfide cross-linking of the MotB protein of *Escherichia coli*: evidence for two H(+) channels in the stator complex. *Biochemistry* 40, 13051–13059
46. Nishikino, T. *et al.* (2020) Characterization of PomA periplasmic loop and sodium ion entering in stator complex of sodium-driven flagellar motor. *J. Biochem. (Tokyo)* 167, 389–398
47. Nishihara, Y. and Kitao, A. (2015) Gate-controlled proton diffusion and protonation-induced ratchet motion in the stator of the bacterial flagellar motor. *Proc. Natl. Acad. Sci. U. S. A.* 112, 7737–7742
48. Takekawa, N. *et al.* (2016) The tetrameric MotA complex as the core of the flagellar motor stator from hyperthermophilic bacterium. *Sci. Rep.* 6, 31526
49. Kühlbrandt, W. (2014) The resolution revolution. *Science* 343, 1443–1444
50. Cheng, Y. (2018) Membrane protein structural biology in the era of single particle cryo-EM. *Curr. Opin. Struct. Biol.* 52, 58–63
51. Lai, Y.-W. *et al.* (2020) Evolution of the stator elements of rotary prokaryote motors. *J. Bacteriol.* 202, e00557-19
52. Ratliff, A.C. *et al.* (2021) Ton motor complexes. *Curr. Opin. Struct. Biol.* 67, 95–100
53. Celia, H. *et al.* (2019) Cryo-EM structure of the bacterial Ton motor subcomplex ExbB–ExbD provides information on structure and stoichiometry. *Commun. Biol.* 2, 1–6
54. Hennell James, R. *et al.* (2021) Structure and mechanism of the proton-driven motor that powers type 9 secretion and gliding motility. *Nat. Microbiol.* 6, 221–233
55. Young, K.T. *et al.* (2007) *Campylobacter jejuni*: molecular biology and pathogenesis. *Nat. Rev. Microbiol.* 5, 665–679
56. Stolz, B. and Berg, H.C. (1991) Evidence for interactions between MotA and MotB, torque-generating elements of the flagellar motor of *Escherichia coli*. *J. Bacteriol.* 173, 7033–7037
57. Morimoto, Y.V. *et al.* (2010) Proton-conductivity assay of plugged and unplugged MotA/B proton channel by

cytoplasmic pHluorin expressed in *Salmonella*. *FEBS Lett.* 584, 1268–1272
58. Onoue, Y. *et al.* (2019) Essential ion binding residues for Na + flow in stator complex of the *Vibrio flagellar* motor. *Sci. Rep.* 9, 11216
59. Sudo, Y. *et al.* (2009) Comparative study of the ion flux pathway in stator units of proton- and sodium-driven flagellar motors. *Biophysics* 5, 45–52
60. Terauchi, T. *et al.* (2011) A conserved residue, PomB-F22, in the transmembrane segment of the flagellar stator complex, has a critical role in conducting ions and generating torque. *Microbiology* 157, 2422–2432
61. Kojima, S. and Blair, D.F. (2001) Conformational change in the stator of the bacterial flagellar motor. *Biochemistry* 40, 13041–13050
62. Spanner, K. (2006) Survey of the various operating principles of ultrasonic piezomotors. In *Actuator 2006: 10th International Conference on New Actuators & 4th International Exhibition on Smart Actuators and Drive Systems* (Borgmann, H., ed.), VG Hanseatische Veranstaltungs-GmbH Division Messe Bremen
63. Ryu, W.S. *et al.* (2000) Torque-generating units of the flagellar motor of *Escherichia coli* have a high duty ratio. *Nature* 403, 444–447
64. Takekawa, N. *et al.* (2020) Structure and energy-conversion mechanism of the bacterial Na+-driven flagellar motor. *Trends Microbiol.* 28, 719–731
65. Terahara, N. *et al.* (2008) Mutations alter the sodium versus proton use of a *Bacillus clausii* flagellar motor and confer dual ion use on *Bacillus subtilis* motors. *Proc. Natl. Acad. Sci. U. S. A.* 105, 14359–14364
66. Ridone, P. *et al.* (2021) Spontaneous adaptation of ion selectivity in a bacterial flagellar motor. *BioRxiv* Published online January 27, 2021. https://doi.org/10.1101/2021.01.26.427765
67. Khan, I.H. *et al.* (1992) The cytoplasmic component of the bacterial flagellar motor. *Proc. Natl. Acad. Sci. U. S. A.* 89, 5956–5960
68. Sircar, R. *et al.* (2013) Structure and activity of the flagellar rotor protein FliY: a member of the CheC phosphatase family. *J. Biol. Chem.* 288, 13493–13502
69. Cheng, C. *et al.* (2018) Flagellar basal body structural proteins FlhB, FliM, and FliY are required for flagellar-associated protein expression in *Listeria monocytogenes*. *Front. Microbiol.* 9, 208
70. Henderson, L.D. *et al.* (2020) Diversification of *Campylobacter jejuni* flagellar C-ring composition impacts its structure and function in motility, flagellar assembly, and cellular processes. *mBio* 11, e02286-19
71. Brown, P.N. *et al.* (2002) Crystal structure of the middle and C-terminal domains of the flagellar rotor protein FliG. *EMBO J.* 21, 3225–3234
72. Minamino, T. *et al.* (2011) Structural insight into the rotational switching mechanism of the bacterial flagellar motor. *PLoS Biol.* 9, e1000616
73. Lee, L.K. *et al.* (2010) Structure of the torque ring of the flagellar motor and the molecular basis for rotational switching. *Nature* 466, 996–1000
74. Xue, C. *et al.* (2018) Crystal structure of the FliF–FliG complex from *Helicobacter pylori* yields insight into the assembly of the motor MS-C ring in the bacterial flagellum. *J. Biol. Chem.* 293, 2066–2078
75. Johnson, S. *et al.* (2020) Symmetry mismatch in the MS-ring of the bacterial flagellar rotor explains the structural coordination of secretion and rotation. *Nat. Microbiol.* 5, 966–975
76. Thomas, D.R. *et al.* (1999) Rotational symmetry of the C ring and a mechanism for the flagellar rotary motor. *Proc. Natl. Acad. Sci. U. S. A.* 96, 10134–10139
77. Thomas, D.R. *et al.* (2006) The three-dimensional structure of the flagellar rotor from a clockwise-locked mutant of *Salmonella enterica* serovar typhimurium. *J. Bacteriol.* 188, 7039–7048
78. Park, S.-Y. *et al.* (2006) Structure of FliM provides insight into assembly of the switch complex in the bacterial flagella motor. *Proc. Natl. Acad. Sci. U. S. A.* 103, 11886–11891
79. Lam, K.-H. *et al.* (2013) Structural basis of FliG–FliM interaction in *Helicobacter pylori*. *Mol. Microbiol.* 88, 798–812
80. Dos Santos, R.N. *et al.* (2018) Characterization of C-ring component assembly in flagellar motors from amino acid coevolution. *R. Soc. Open Sci.* 5, 171854
81. Terashima, H. *et al.* (2021) Site-directed crosslinking identifies the stator-rotor interaction surfaces in a hybrid bacterial flagellar motor. *J. Bacteriol.* Published online April 8, 2021. https://doi.org/10.1128/JB.00016-21
82. Zhou, J. and Blair, D.F. (1997) Residues of the cytoplasmic domain of MotA essential for torque generation in the bacterial flagellar motor. *J. Mol. Biol.* 273, 428–439
83. Zhou, J. *et al.* (1998) Electrostatic interactions between rotor and stator in the bacterial flagellar motor. *Proc. Natl. Acad. Sci. U. S. A.* 95, 6436–6441
84. Morimoto, Y.V. *et al.* (2010) Charged residues in the cytoplasmic loop of MotA are required for stator assembly into the bacterial flagellar motor. *Mol. Microbiol.* 78, 1117–1129
85. Yakushi, T. *et al.* (2006) Roles of charged residues of rotor and stator in flagellar rotation: comparative study using H+-driven and Na+-driven motors in *Escherichia coli*. *J. Bacteriol.* 188, 1466–1472
86. Takekawa, N. *et al.* (2014) Contribution of many charged residues at the stator-rotor interface of the Na+-driven flagellar motor to torque generation in *Vibrio alginolyticus*. *J. Bacteriol.* 196, 1377–1385
87. Reid, S.W. *et al.* (2006) The maximum number of torque-generating units in the flagellar motor of *Escherichia coli* is at least 11. *Proc. Natl. Acad. Sci. U. S. A.* 103, 8066–8071
88. Leake, M.C. *et al.* (2006) Stoichiometry and turnover in single, functioning membrane protein complexes. *Nature* 443, 355–358
89. Lele, P.P. *et al.* (2013) Dynamics of mechanosensing in the bacterial flagellar motor. *Proc. Natl. Acad. Sci. U. S. A.* 110, 11839–11844
90. Tipping, M.J. *et al.* (2013) Load-dependent assembly of the bacterial flagellar motor. *mBio* 4, e00551-13
91. Nord, A.L. *et al.* (2017) Catch bond drives stator mechanosensitivity in the bacterial flagellar motor. *Proc. Natl. Acad. Sci. U. S. A.* 114, 12952–12957
92. Wadhwa, N. *et al.* (2019) Torque-dependent remodeling of the bacterial flagellar motor. *Proc. Natl. Acad. Sci. U. S. A.* 116, 11764–11769
93. Wadhwa, N. *et al.* (2021) Mechanosensitive remodeling of the bacterial flagellar motor is independent of direction of rotation. *Proc. Natl. Acad. Sci. U. S. A.* 118, e2024608118
94. Minamino, T. *et al.* (2019) Directional switching mechanism of the bacterial flagellar motor. *Comput. Struct. Biotechnol. J.* 17, 1075–1081
95. Kudo, S. *et al.* (2005) Asymmetric swimming pattern of *Vibrio alginolyticus* cells with single polar flagella. *FEMS Microbiol. Lett.* 242, 221–225
96. Charon, N.W. *et al.* (2012) The unique paradigm of spirochete motility and chemotaxis. *Annu. Rev. Microbiol.* 66, 349–370
97. Pilizota, T. *et al.* (2009) A molecular brake, not a clutch, stops the *Rhodobacter sphaeroides* flagellar motor. *Proc. Natl. Acad. Sci. U. S. A.* 106, 11582–11587
98. Attmannspacher, U. *et al.* (2005) Control of speed modulation (chemokinesis) in the unidirectional rotary motor of *Sinorhizobium meliloti*. *Mol. Microbiol.* 56, 708–718
99. Stock, D. *et al.* (2012) Nanorotors and self-assembling macromolecular machines: the torque ring of the bacterial flagellar motor. *Curr. Opin. Biotechnol.* 23, 545–554
100. Wadhams, G.H. and Armitage, J.P. (2004) Making sense of it all: bacterial chemotaxis. *Nat. Rev. Mol. Cell Biol.* 5, 1024–1037
101. Parkinson, J.S. *et al.* (2015) Signaling and sensory adaptation in *Escherichia coli* chemoreceptors: 2015 update. *Trends Microbiol.* 23, 257–266
102. Atsumi, T. *et al.* (1992) Polar and lateral flagellar motors of marine *Vibrio* are driven by different ion-motive forces. *Nature* 355, 182–184
103. Paul, K. *et al.* (2010) The c-di-GMP binding protein YcgR controls flagellar motor direction and speed to affect chemotaxis by a 'backstop brake' mechanism. *Mol. Cell* 38, 128–139
104. Boehm, A. *et al.* (2010) Second messenger-mediated adjustment of bacterial swimming velocity. *Cell* 141, 107–116